Int. J. Electrochem. Sci., 15 **(2020)** 12587 – 12598, doi: 10.20964/2020.12.62

International Journal of
ELECTROCHEMICAL
SCIENCE
www.electrochemsci.org

Electrochemical Determination of Methandrostenolone Using a Molecularly Imprinted Sensor

Linlin Shan

College of Physical Education, Zhengzhou University of Science and Technology, Zhengzhou, Henan 450064, China
E-mail: linlinshan@sutcm.net

Received: 1 July 2020 / *Accepted:* 28 September 2020 / *Published:* 31 October 2020

Anabolic androgenic steroids have a chemical structure similar to that of testosterone and are the most commonly abused and most frequently used sports stimulants. This work proposes a simple methandrostenolone electrochemical sensor based on a nanocomposite with the assistance of molecular imprinting technology. Three-dimensional Au nanowires (AuNWs) were first synthesized using an ionic liquid (IL) as the guiding agent. The adhesion properties of the IL are used to fix Pt nanoparticles to obtain PtNPs/AuNWs/IL. At the same time, the PtNPs/AuNWs/IL nanocomposite was loaded on the surface of a carboxylated reduced graphene oxide-modified electrode. Then, the methandrostenolone electrochemical sensor was constructed by electropolymerization of o-phenylenediamine with the imprinting of metandienone.

Keywords: Electrochemical sensor; Metandienone; Voltammetric determination; Molecular imprinted sensor; Stimulant

1. INTRODUCTION

Anabolic androgenic steroids have a chemical structure similar to that of testosterone and are the most commonly abused and most frequently used sports stimulants [1–3]. In 1974, the International Olympic Committee added anabolic androgenic steroids as stimulants to the list of prohibited substances and stipulated that anabolic androgenic steroids were banned on all occasions. Methandrostenolone is a protein assimilation hormone that can obviously promote protein synthesis and assimilation and simultaneously reduce amino acid decomposition and dissimilation [4–7]. Methandrostenolone can increase muscle growth, increase body weight, reduce azotaemia, and promote bone marrow haematopoietic function. This hormone is mainly used to treat the symptoms of protein assimilation, insufficient absorption, excessive protein breakdown and excessive loss [8–11].

At present, the test standard for methandrostenolone prescribed by the International Olympic Committee is the analysis of urine samples by GC/MS. Since anabolic androgenic steroids in urine samples mainly exist in the form of metabolites, the targets of detection are molecules and their metabolites [12,13]. Urinary tests for methandrostenolone currently have certain disadvantages, such as the privacy of urine collection, test time limit, storage, and the distinction between exogenous and endogenous substances. The detection of anabolic androgenic steroid stimulants by other biological samples such as blood, sweat, saliva, hair, nails, and foetal urine has also been reported in the literature. Hair is increasingly used because of its advantages of stability, simple sample collection process, easy storage, long detection time limit, and reflection of medication history [14–18]. On the other hand, the development of analytical techniques has also shown an alternative approach for methandrostenolone detection.

In the construction of electrochemical sensors, researchers often use biological substances with recognition functions (such as enzymes, antibodies, nucleic acids, cells, and microorganisms) that exist in nature to improve the selectivity and sensitivity of sensors [19–21]. However, the biometric unit is easily deactivated in acids, alkalis, organic solvents, or environments such as ultrasound, limiting its application [22,23]. To this end, researchers have investigated and obtained inexpensive and stable molecularly imprinted polymers (MIPs), which are used as new identification elements for the development of electrochemical sensors [24,25]. This type of polymer recognition element not only has a characteristic recognition capability comparable to that of a biometric recognition unit but also has better chemical and physical stability than a biometric recognition unit. At the same time, MIPs have the advantages of inexpensive raw materials, easy availability and reusability. Therefore, MIPs represent a kind of recognition element with very good application prospects.

At present, electrochemical sensors based on molecular imprinting have been widely used for the determination of small organic molecules such as drug molecules and food additives as well as biological macromolecules such as peptides and proteins [26–28]. Detection methods include chronoamperometry, differential pulse voltammetry, and electrochemical impedance spectroscopy. Investigations have found that the preparation of MIP electrodes is a key factor affecting the performance of molecularly imprinted electrochemical sensors. At present, there are two main methods for preparing MIP membrane electrodes [29–35]. One approach is in situ surface imprinting polymerization under conditions of light, heating or voltage application to obtain MIP-modified electrodes. The second approach is to use conductive adhesives to convert organic radicals. The MIP obtained by the initiation polymerization method or the sol-gel polymerization method is fixed to the electrode surface. In the in situ surface imprinting polymerization method, the electropolymerization method has the advantages of simple preparation, uniform film thickness and controllability. In addition, in the construction of this type of sensor, the imprinted substrate is an important factor affecting the performance [36,37]. Commonly used imprinted substrates include metal nanomaterials, r-GO, MWCNTs, TiO_2 and sol-gel films. These materials can enable MIPs to obtain more effective imprinting sites. However, these modified electrodes are usually two-dimensional modified interfaces, and there are certain limitations in mass transfer and signal transmission. Compared with the two-dimensional nano-membrane, the three-dimensional membrane-modified electrode has a larger surface area and a higher mass transfer rate, which is very beneficial for constructing an electrochemical molecularly imprinted sensor with high sensitivity and selectivity.

In this work, using an IL ([BMIM][BF_4]) as the structure-directing agent and sodium citrate as the reducing agent, AuNWs/IL was prepared in one step. Using the IL in AuNWs/IL to load PtNPs in its network, a three-dimensional porous modified electrode was obtained. The composite material was then applied onto a carboxylated reduced graphene oxide (CrGO)-modified GCE. Then, using this as the electropolymerization substrate, o-phenylenediamine (PD) as the functional monomer, and metandienone as the template molecule, the MIP membrane-modified electrode was prepared by the cyclic voltammetry (CV) method. This method increases the number of effective imprinting sites and improves the electron transfer capabilities of the MIP membrane, thereby making the sensor more sensitive.

2. EXPERIMENTAL

All reagents, including [BMIM][BF_4], $H_2PtCl_6 \cdot 6H_2O$, $HAuCl_4 \cdot 4H_2O$, o-phenylenediamine (PD), ascorbic acid, KH_2PO_4, and Na_2HPO_4, were purchased from Macklin Co., Ltd. and used without purification. Metandienone was purchased from Nanin Youshan Biotech Co., Ltd. The working electrode, counter electrode and reference electrode were glassy carbon, Pt wire and Ag/AgCl (3 M), respectively. Phosphate buffer solution (PBS) was prepared by mixing stock solutions of 0.1 M disodium hydrogen phosphate and sodium dihydrogen phosphate. The electrochemical determination of metandienone was carried out using a CHI760 electrochemical workstation. Differential pulse voltammetry (DPV) was used for electrochemical recording. The scan range was 0.2–0.9 V, the pulse amplitude was 50 mV, the pulse width was 0.05 s and the pulse period was 0.5 s.

AuNWs/IL was prepared using the following process: 400 μL of $HAuCl_4 \cdot 4H_2O$ (25 mM), 25 μL of [BMIM][BF_4] and 5 mL of H_2O were added to a beaker and heated to 100 °C under stirring. Then, 3 mL of ascorbic acid (20 mM) was added and reacted for 30 min. The AuNWs/IL was then collected after a simple filtration process.

PtNPs were prepared using the following process: 0.05 mL of KOH (1 M) and 0.01 mL of ascorbic acid (20 mM) were added into 2 mL of H_2O. Then, 4 mL of $H_2PtCl_6 \cdot 6H_2O$ (5 mM) was added into the above solution and reacted at 60 °C under stirring for 30 min. PtNPs were then collected after a simple filtration process.

PtNPs/AuNWs/IL was prepared by adding 10 mg of PtNPs into 1 mL of AuNW/IL dispersion with sonication.

Electrode modification: First, 5 μL of CrGO was dip-coated on a GCE and dried naturally. Then, 5 μL of PtNPs/AuNWs/IL was dip-coated on a GCE and dried naturally to form PtNPs/AuNWs/IL/CrGO/GCE.

MIP sensor preparation: A PtNPs/AuNWs/IL/CrGO/GCE was immersed into a PBS solution containing 0.4 mM PD and 0.1 mM metandienone. Then, a CV scan was conducted from 0-1.2 V for 5 cycles. Next, the electrode was dried naturally. The dried electrode was immersed in HCl (0.1 M) solution for a 30 min elution process. The prepared MIP sensor was denoted as MIP/PtNPs/AuNWs/IL/CrGO/GCE.

3. RESULTS AND DISCUSSION

Figure 1 shows a schematic diagram depicting the stepwise preparation process of the MIP/PtNPs/AuNWs/IL/CrGO/GCE. Bulk solution free radical polymerization is a classic method for preparing MIPs. Generally, template molecules, functional monomers, cross-linking agents and initiators are added to an appropriate polymerization solvent. Under an applied voltage, the polymerization reaction is initiated to obtain a bulk polymer [38–40]. After eluting the template molecule, the MIP is obtained. Organic radical-initiated polymerization is a complex reaction process. In addition to the polymerization method, the performance of the resulting MIP is affected by the polymerization conditions such as template molecules, functional monomers, cross-linking agents, reaction solvents, and initiation methods. The ideal template molecule should have good chemical stability, multiple recognition groups and no inhibitory groups, for example, environmental hormones, drug molecules (pesticides, veterinary drugs and antibiotics, etc.) and heavy metal ions [41,42].

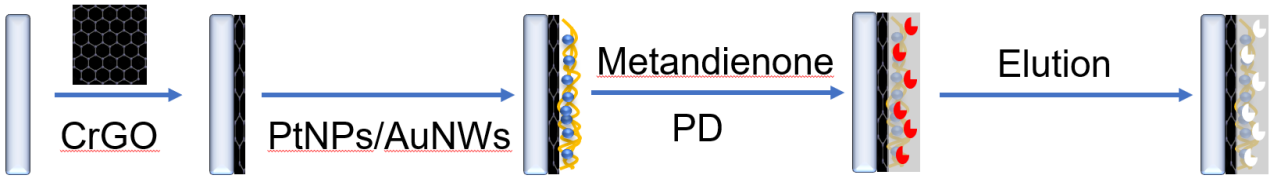

Figure 1. Schematic diagram of the stepwise preparation process of the MIP/PtNPs/AuNWs/IL/CrGO/GCE.

The experiment records the EIS diagram reflecting the change process of the electrode modification interface. As shown in Figure 2A, the GCE has a small semicircle in the high-frequency stage, indicating that its electron transfer ability is low, and the impedance value is approximately 1074 Ω. When the GCE is modified by CrGO, its impedance value drops to approximately 544 Ω. This result shows that CrGO improves the electron transfer ability of the electrode. When the CrGO/GCE was modified by PtNPs, the electrode impedance value further decreased to 322 Ω, indicating that PtNPs further improved the electron transfer capability of the modified interface. When PtNPs are attached to AuNWs/IL, the impedance of the resulting PtNPs/AuNWs/IL/CrGO/GCE shows a straight line, indicating that this electrochemical process is controlled by diffusion, which is due to the excellent electron transport capability of the modified interface. This enhanced performance can result from the electrode surface area and the synergistic effect of PtNPs and AuNWs [43,44].

After PtNPs/AuNWs/IL/CrGO/GCE surface electropolymerization with the imprinted MIP film (Figure 2B), the impedance of the resulting electrode increased to 5700 Ω, indicating that the MIP has a larger resistance. After the template molecules in the MIP membrane were eluted and removed, the impedance value of the resulting electrode dropped to 1070 Ω, indicating that the presence of imprinted hole sites reduced the membrane resistance. However, after being immersed in a 10 μM solution of metandienone and enriched, the resulting electrode impedance increased to 5244 Ω again, indicating that the metandienone molecule occupies the imprinted site, hindering the electrochemistry of the $Fe(CN)_6^{3-/4-}$ probe at the electrode surface.

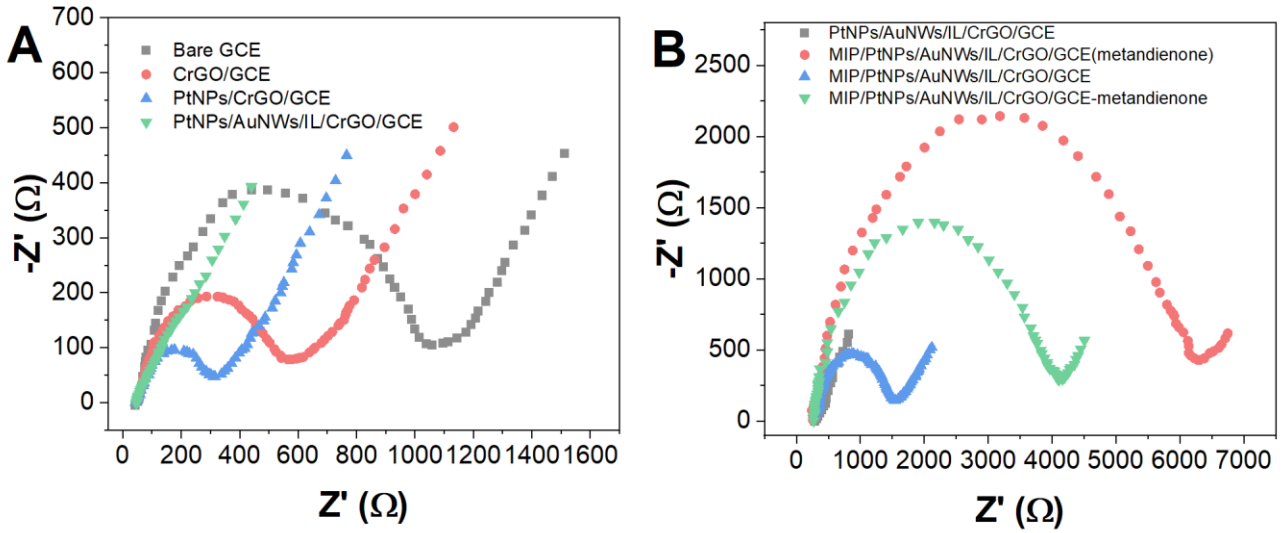

Figure 2. (A) EIS spectra of GCE, CrGO/GCE, PtNPs/CrGO/GCE and PtNPs/AuNWs/IL/CrGO/GCE in 5 mM $K_3Fe(CN)_6$ + $K_4Fe(CN)_6$ containing 0.1 M KCl. (B) EIS spectra of PtNPs/AuNWs/IL/CrGO/GCE, MIP/PtNPs/AuNWs/IL/CrGO/GCE(metandienone), MIP/PtNPs/AuNWs/IL/CrGO/GCE and MIP/PtNPs/AuNWs/IL/CrGO/GCE-metandienone in 5 mM $K_3Fe(CN)_6$ + $K_4Fe(CN)_6$ containing 0.1 M KCl.

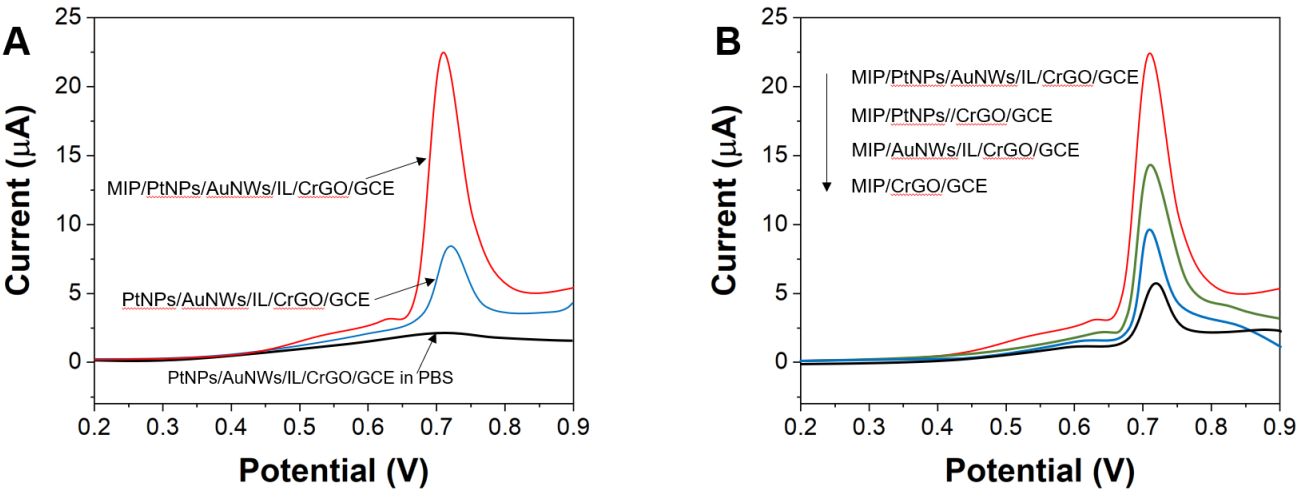

Figure 3. (A) DPV curves of PtNPs/AuNWs/IL/CrGO/GCE and MIP/PtNPs/AuNWs/IL/CrGO/GCE in the presence of 10 uM methandrostenolone , PtNPs/AuNWs/IL/CrGO/GCE in PBS. (B) DPV curves of MIP/CrGO/GCE, MIP/PtNPs/CrGO/GCE, MIP/AuNWs/IL/CrGO/GCE and MIP/PtNPs/AuNWs/IL/CrGO/GCE in the presence of 10 uM methandrostenolone .

DPV was used to investigate the response of different electrodes to metandienone. As shown in Figure 3A, the MIP/PtNPs/AuNWs/IL/CrGO/GCE has no obvious redox peaks in the PBS buffer solution. However, when the MIP/PtNPs/AuNWs/IL/CrGO/GCE was in a 10 μM metandienone solution, an obvious oxidation peak appeared at 740 mV. However, for the PtNPs/AuNWs/IL/CrGO/GCE under the same experimental conditions, the peak current is smaller, indicating that the imprinting effect was obvious. Figure 3B presents the response current of different imprinted sensors to metandienone. The results show that the response current of the

MIP/PtNPs/CrGO/GCE is larger than that of the MIP/CrGO/GCE. The reason may be that PtNPs have a larger specific surface area and higher electron transport capability. In addition, the response current of the MIP/AuNWs/IL/CrGO/GCE is greater than that of the MIP/PtNPs/CrGO/GCE because the three-dimensional structure of AuNWs has a larger specific surface area and facilitates mass transfer. The MIP/PtNPs/AuNWs/IL/CrGO/GCE response current is greater than that of the other three.

Figure 4A shows the effect of different CrGO concentrations on the MIP/PtNPs/AuNWs/IL/CrGO/GCE. When the CrGO concentration is 1 mg/mL, the sensor response current value is the largest. This is because as the concentration increases, the surface area of the electrode increases, resulting in an increased response current. However, when the CrGO concentration is greater than 1 mg/mL, the response current is gradually reduced, which may be related to the increased thickness of the modified electrode film and the increased electron transfer resistance [45–48].

Figure 4B shows the effect of different AuNWs/IL concentrations on the MIP/PtNPs/AuNWs/IL/CrGO/GCE. When the concentration of AuNWs/IL is between 7 and 15 mg/mL, the response current increases as the concentration of AuNWs/IL increases. When the concentration of AuNWs/IL exceeds 15 mg/mL, the response current gradually decreases, which is because the amount of PtNPs attached increases with increasing AuNWs/IL concentration. The amount of PtNPs is fixed so that its ratio in AuNWs/IL decreases, resulting in a decrease in the electron transfer ability of the MIP, so the response current gradually decreases.

Figure 4C shows the effect of different PtNP concentrations on the MIP/PtNPs/AuNWs/IL/CrGO/GCE. It can be seen that as the concentration of PtNPs increases in the range of 5-10 mg/L, the response current increases. When the PtNP concentration exceeds 10 mg/L, the response current gradually decreases, which is the same as that mentioned above. The density of PtNPs in AuNWs/IL is related to changes in the response current.

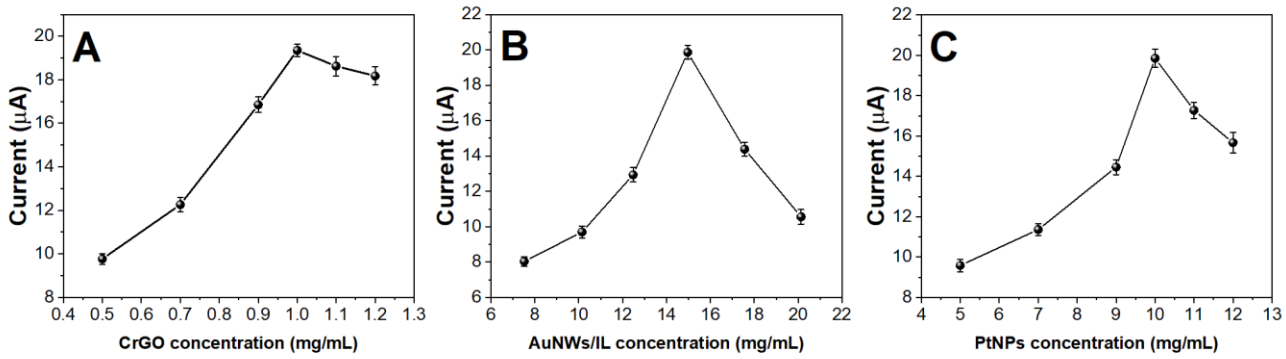

Figure 4. Effect of (A) CrGO concentration, (B) AuNWs/IL concentration and (C) PtNPs concentration on MIP/PtNPs/AuNWs/IL/CrGO/GCE in the presence of 10 uM methandrostenolone. Current values were recorded using DPV.

Figure 5A shows the effect of the resulting sensor on the response current of methandrostenolone when the ratio of template molecules to functional monomers varies between 1:2 and 1:6. As their ratio decreases, the response current gradually increases first and then decreases. When their ratio is 1:4, the

response current reaches a maximum. The reason may be that the change in the ratio of the two monomers caused a change in the number of effective imprinting sites in the MIP membrane [49,50]. When the amount of functional monomers is small, there are few template molecules that can be fixed. Conversely, when too many functional monomers are present, many effective imprinting sites are embedded in the polymer matrix, which reduces the number of effective imprinting sites and the mass transfer rate.

Figure 5B shows the effect of the resulting sensor on the response current of methandrostenolone when the polymerization time is increased from 60 s to 240 s. It can be seen that when the polymerization time changes from 60 to 140 s, the response current increases with the polymerization time. However, when the polymerization time exceeds 140 s, the response current gradually decreases. This result is due to the increase in the polymerization time, which results in an increased thickness of the imprinted film, an increased resistance of the imprinted film, and a reduced number of effective imprinted sites.

Figure 5C presents the effect of the MIP/PtNPs/AuNWs/IL/CrGO/GCE on the response current of methandrostenolone as the accumulation time changes. When the concentration of methandrostenolone is high and the accumulation time is 50~300 s, the response current gradually increases first and then remains basically unchanged, indicating that the adsorption of methandrostenolone reaches equilibrium. When the concentration of methandrostenolone is low, the adsorption equilibrium time is extended to 350 s. To achieve a lower concentration of methandrostenolone adsorption equilibrium on the MIP membrane electrode, the 500 s was selected as the accumulation time.

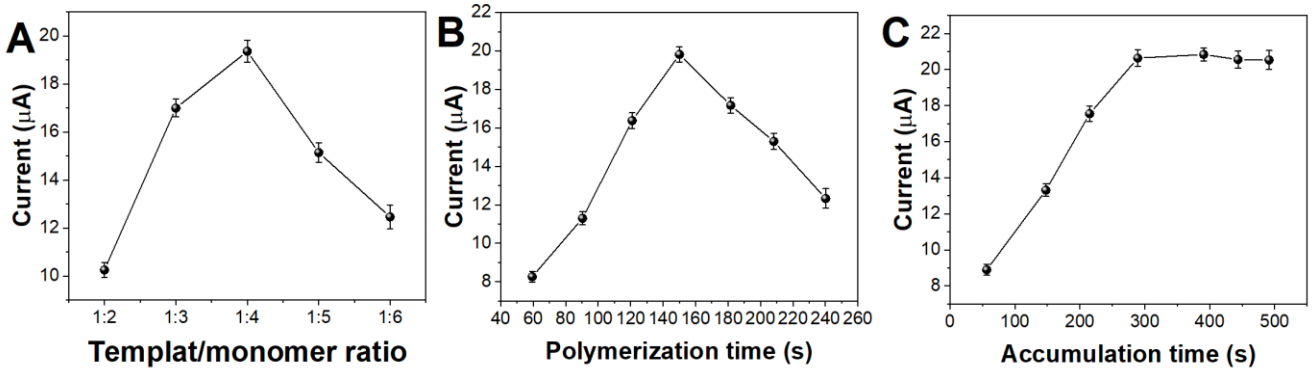

Figure 5. Effect of (A) ratio of template molecules to functional monomers, (B) polymerization time and (C) accumulation time on MIP/PtNPs/AuNWs/IL/CrGO/GCE in the presence of 10 uM methandrostenolone . Current values were recorded using DPV.

The pH of the electrolyte solution is an important parameter for the measurement of metandienone by the sensor. The experiment found that when the pH value changes from 1.9 to 4.5, the MIP/PtNPs/AuNWs/IL/CrGO/GCE response current to methandrostenolone changes correspondingly, as shown in Figure 6A, and the optimal pH is 2. In addition, the peak potential moves with the change in pH, and the slope of the curve between the peak potential and pH is -53.4 mV/pH (Figure 6B),

indicating that the number of protons and electrons participating in this electrochemical reaction is equal. The possible electrochemical oxidation mechanism is shown in Figure 7.

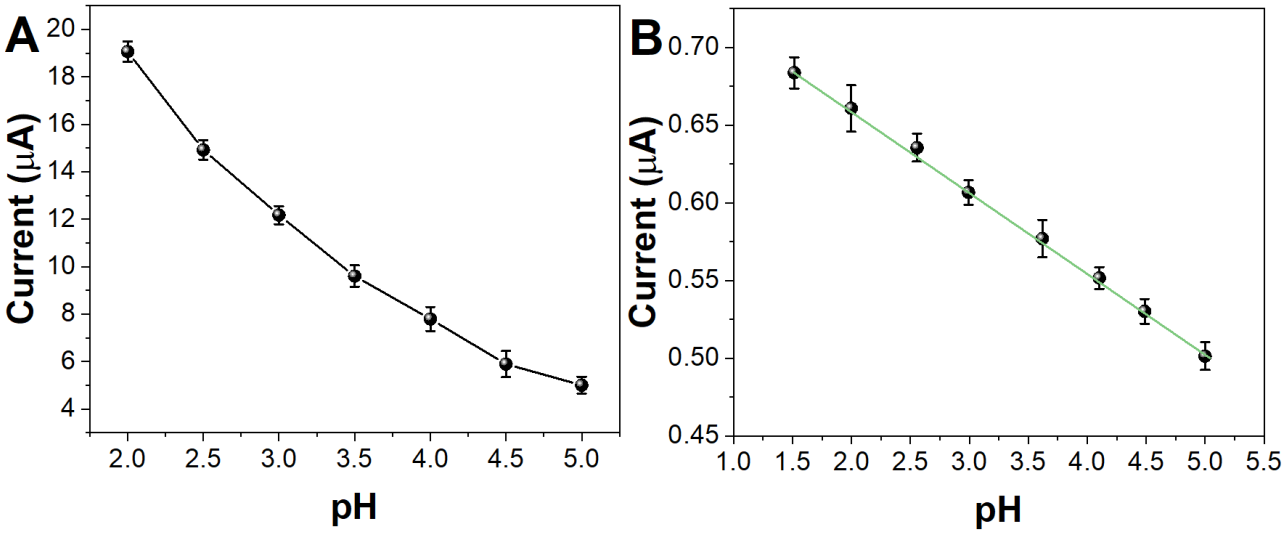

Figure 6. (A) Effect of pH on MIP/PtNPs/AuNWs/IL/CrGO/GCE towards in the presence of 10 uM methandrostenolone. (B) Plots of the peak potentials vs. pH conditions.

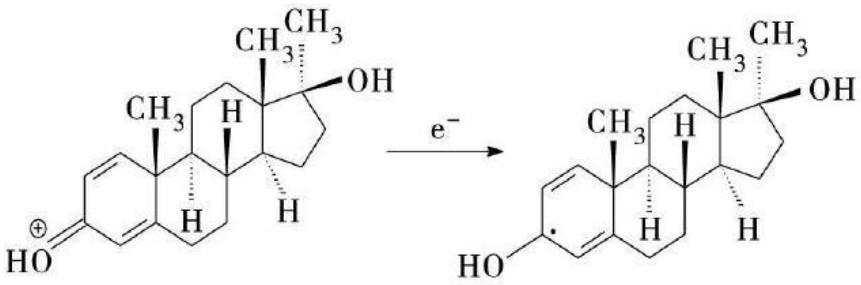

Figure 7. Electrochemical oxidation process of methandrostenolone.

Under the optimized experimental conditions, the DPV curve of the sensor's response to methandrostenolone was recorded (Figure 7). As expected, the response current of the DPV increases with increasing metandienone concentration, with a linear range of 2 nM-9.6 μM. The lower detection limit is 0.4 nM (S/N=3).

To discuss the selectivity of the MIP/PtNPs/AuNWs/IL/CrGO/GCE, five common biomolecules that may interfere with the actual detection of methandrostenolone were investigated in this experiment, as shown in Figure 8. The results show that when the concentrations of glucose, uric acid, glutamic acid, clenbuterol and boldenone are 10 times higher than that of metandienone, there is no obvious interference with the actual detection of metandienone. Therefore, the proposed sensor exhibited an excellent anti-interference property.

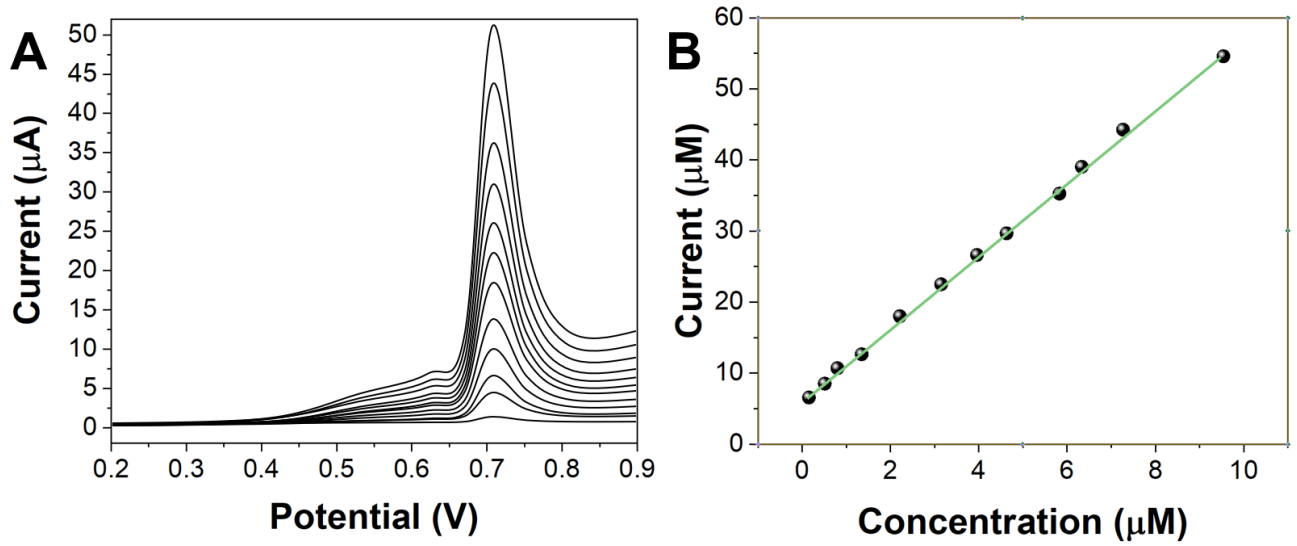

Figure 8. (A) DPV curves of MIP/PtNPs/AuNWs/IL/CrGO/GCE towards different concentrations of methandrostenolone. (B) Plots of the peak current vs. concentrations of metadienone.

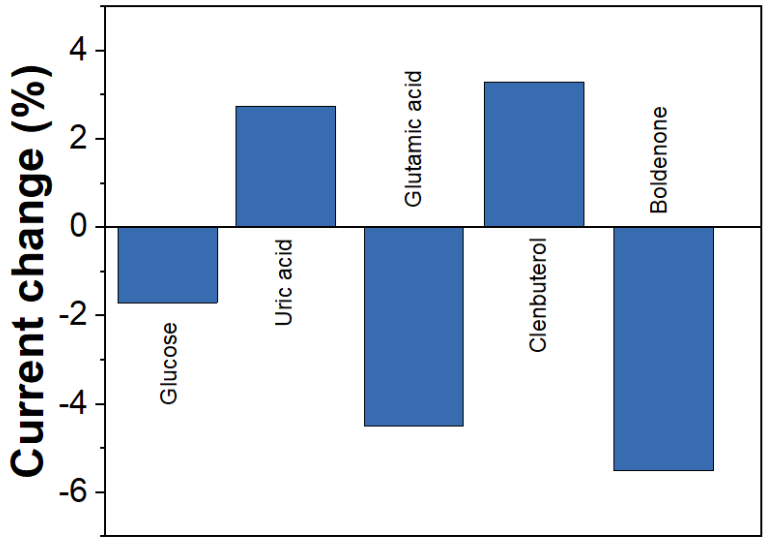

Figure 9. Anti-interference property of the MIP/PtNPs/AuNWs/IL/CrGO/GCE.

The obtained sensor was used for 5 parallel determinations of metandienone, and the relative standard deviation (RSD) of the response peak current value was 7.7%. To evaluate the stability of the sensor, the measurement of methandrostenolone 15 consecutive times showed that the response current value of the sensor remained at 96.6% of the initial value. Additionally, the sensor was placed at room temperature for 20 days, and when the methandrostenolone was measured again, its response value remained at 95.7% of the initial value, indicating that the sensor has good stability.

Methandrostenolone content tests were performed in spiked serum samples to evaluate the feasibility of using the MIP/PtNPs/AuNWs/IL/CrGO/GCE. For the serum samples, the accuracy of the experimental results is expressed in terms of recovery (Table 1).

Table 1. Results of methandrostenolone determination in serum samples under optimal conditions.

Sample	Added (uM)	Found (uM)	Recovery (%)	RSD (%)
Serum 1	3.00	2.97	99.00	4.21
Serum 2	5.00	5.04	100.80	3.55
Serum 3	7.00	7.11	101.57	4.25

4. CONCLUSION

This work proposes a simple solution method to prepare three-dimensional AuNWs/IL, in which IL not only is the guiding agent for Au to grow into a three-dimensional structure but also tightly adheres to the surface of AuNWs. The adhesion properties of the IL are used to fix PtNPs on AuNWs to obtain PtNPs/AuNWs/IL. At the same time, PtNPs/AuNWs/IL was loaded on the surface of a CrGO-modified electrode, and then, the methandrostenolone electrochemical sensor with high sensitivity and high selectivity was constructed by electropolymerization of PD with the imprinting of methandrostenolone.

References

1. D.B. da J. Neves, E.D. Caldas, *Forensic Sci. Int.*, 275 (2017) 272–281.
2. H. Dahmani, K. Louati, A. Hajri, S. Bahri, F. Safta, *Steroids*, 138 (2018) 134–160.
3. B.D. Anawalt, *Use Abuse Anab. Horm. Androg. Beyond*, 464 (2018) 21–27.
4. M. Thevis, K. Walpurgis, A. Thomas, *Anal. Chem.*, 92 (2020) 506–523.
5. X. TAN, Z. LI, L. DENG, S. ZHAO, M. WANG, *J. Integr. Agric.*, 15 (2016) 2163–2174.
6. D.Yu. Shostko, A.I. Liubina, Yu.Yu. Kozyrkov, S.A. Beliaev, *Steroids*, 158 (2020) 108601.
7. M. Raro, T. Portolés, E. Pitarch, J.V. Sancho, F. Hernández, L. Garrostas, J. Marcos, R. Ventura, J. Segura, O.J. Pozo, *Anal. Chim. Acta*, 906 (2016) 128–138.
8. T. Piper, W. Schänzer, M. Thevis, *LC-MS Based Anal. Appl. Steroid Res.*, 162 (2016) 80–91.
9. S. Lehmann, A. Thomas, K.-H. Schiwy-Bochat, H. Geyer, M. Thevis, F. Glenewinkel, M.A. Rothschild, H. Andresen-Streichert, M. Juebner, *Forensic Sci. Int.*, 303 (2019) 109925.
10. N. Kratena, V.S. Enev, G. Gmeiner, P. Gärtner, *Steroids*, 115 (2016) 75–79.
11. G. Forsdahl, K. Zanitzer, D. Erceg, G. Gmeiner, *Steroids*, 157 (2020) 108614.
12. Y. Liu, J. Lu, S. Yang, Q. Zhang, Y. Xu, *Steroids*, 108 (2016) 61–67.
13. P. Kintz, *Toxicol. Anal. Clin.*, 29 (2017) 320–324.
14. X. Wang, S.S. Johansen, M.K.K. Nielsen, K. Linnet, *Forensic Sci. Int.*, 285 (2018) e1–e12.
15. M. del M. Ramírez Fernández, S.M.R. Wille, V. Di Fazio, N. Samyn, *Forensic Sci. Int.*, 302 (2019) 109864.

16. J.J. Palamar, A. Salomone, M. Vincenti, C.M. Cleland, *Drug Alcohol Depend.*, 161 (2016) 200–205.
17. S.S. Johansen, *Forensic Sci. Int.*, 270 (2017) e12–e15.
18. G. Frison, S. Frasson, F. Zancanaro, G. Tedeschi, L. Zamengo, *Spec. Issue 53rd Annu. Meet. Int. Assoc. Forensic Toxicol. TIAFT*, 265 (2016) 131–137.
19. F.M. Zahed, B. Hatamluyi, F. Lorestani, Z. Es'haghi, *J. Pharm. Biomed. Anal.*, 161 (2018) 12–19.
20. N.P. Shetti, S.J. Malode, D.S. Nayak, T.M. Aminabhavi, K.R. Reddy, *Microchem. J.*, 150 (2019) 104124.
21. Y. Panahi, A. Motaharian, M.R.M. Hosseini, O. Mehrpour, *Sens. Actuators B Chem.*, 273 (2018) 1579–1586.
22. B. Mutharani, P. Ranganathan, S.-M. Chen, *Sens. Actuators B Chem.*, 304 (2020) 127361.
23. Y. Liu, M. Wei, Y. Hu, L. Zhu, J. Du, *Sens. Actuators B Chem.*, 255 (2018) 544–551.
24. F. Cao, Q. Dong, C. Li, J. Chen, X. Ma, Y. Huang, D. Song, C. Ji, Y. Lei, *Sens. Actuators B Chem.*, 256 (2018) 143–150.
25. S. Ansari, M.S. Ansari, S.P. Satsangee, R. Jain, *Anal. Chim. Acta*, 1046 (2019) 99–109.
26. M.L. Yola, N. Atar, *J. Electrochem. Soc.*, 164 (2017) B223–B229.
27. H. Rao, M. Chen, H. Ge, Z. Lu, X. Liu, P. Zou, X. Wang, H. He, X. Zeng, Y. Wang, *Biosens. Bioelectron.*, 87 (2017) 1029–1035.
28. P. Palladino, F. Bettazzi, S. Scarano, *Anal. Bioanal. Chem.*, 411 (2019) 4327–4338.
29. J. Liu, Y. Zhang, M. Jiang, L. Tian, S. Sun, N. Zhao, F. Zhao, Y. Li, *Biosens. Bioelectron.*, 91 (2017) 714–720.
30. Y. Lai, Y. Deng, G. Yang, S. Li, C. Zhang, X. Liu, *J. Biomed. Nanotechnol.*, 14 (2018) 1688–1694.
31. M. Zhang, B. Pan, Y. Wang, X. Du, L. Fu, Y. Zheng, F. Chen, W. Wu, Q. Zhou, S. Ding, *ChemistrySelect*, 5 (2020) 5035–5040.
32. Y. Xu, Y. Lu, P. Zhang, Y. Wang, Y. Zheng, L. Fu, H. Zhang, C.-T. Lin, A. Yu, *Bioelectrochemistry*, 133 (2020) 107455.
33. L. Fu, K. Xie, A. Wang, F. Lyu, J. Ge, L. Zhang, H. Zhang, W. Su, Y.-L. Hou, C. Zhou, *Anal. Chim. Acta*, 1081 (2019) 51–58.
34. L. Fu, Q. Wang, M. Zhang, Y. Zheng, M. Wu, Z. Lan, J. Pu, H. Zhang, F. Chen, W. Su, *Front. Chem.*, 8 (2020) 92.
35. X. Zhang, R. Yang, Z. Li, M. Zhang, Q. Wang, Y. Xu, L. Fu, J. Du, Y. Zheng, J. Zhu, *Rev. Mex. Ing. Quím.*, 19 (2020) 281–291.
36. G. Bolat, Y.T. Yaman, S. Abaci, *Sens. Actuators B Chem.*, 299 (2019) 127000.
37. O.S. Ahmad, T.S. Bedwell, C. Esen, A. Garcia-Cruz, S.A. Piletsky, *Trends Biotechnol.*, 37 (2019) 294–309.
38. Q. Wang, R. Xue, H. Guo, Y. Wei, W. Yang, *J. Electroanal. Chem.*, 817 (2018) 184–194.
39. P. Jolly, V. Tamboli, R.L. Harniman, P. Estrela, C.J. Allender, J.L. Bowen, *Biosens. Bioelectron.*, 75 (2016) 188–195.
40. L. Fu, A. Wang, K. Xie, J. Zhu, F. Chen, H. Wang, H. Zhang, W. Su, Z. Wang, C. Zhou, *Sens. Actuators B Chem.*, 304 (2020) 127390.
41. J. Huang, Y. Wu, J. Cong, J. Luo, X. Liu, *Sens. Actuators B Chem.*, 259 (2018) 1–9.
42. X. Chen, S. Zhang, X. Shan, Z. Chen, *Anal. Chim. Acta*, 1072 (2019) 54–60.
43. M.L. Yola, C. Göde, N. Atar, *Electrochimica Acta*, 246 (2017) 135–140.
44. M.L. Yola, N. Atar, *J. Electrochem. Soc.*, 164 (2017) B223–B229.
45. V.V. Shumyantseva, T.V. Bulko, L.V. Sigolaeva, A.V. Kuzikov, P.V. Pogodin, A.I. Archakov, *Biosens. Bioelectron.*, 99 (2018) 216–222.
46. M. Torkashvand, M.B. Gholivand, Gh. Malekzadeh, *Sens. Actuators B Chem.*, 231 (2016) 759–767.
47. A. Nezhadali, M. Mojarrab, *Anal. Chim. Acta*, 924 (2016) 86–98.

48. L. Fu, Y. Zheng, P. Zhang, H. Zhang, Y. Xu, J. Zhou, H. Zhang, H. Karimi-Maleh, G. Lai, S. Zhao, *Biosens. Bioelectron.* (2020) 112212.
49. Y. Li, C. Jiang, *Biosens. Bioelectron.*, 119 (2018) 18–24.
50. C. Pelin Böke, O. Karaman, H. Medetalibeyoglu, C. Karaman, N. Atar, M. Lütfi Yola, *Microchem. J.*, 157 (2020) 105012.